

An All-digital 8.6-nJ/Frame 65-nm Tsetlin Machine Image Classification Accelerator

Svein Anders Tunheim[✉], *Senior Member, IEEE*, Yujin Zheng[✉], Lei Jiao[✉], *Senior Member, IEEE*,
Rishad Shafik[✉], *Senior Member, IEEE*, Alex Yakovlev[✉], *Fellow, IEEE*, and Ole-Christoffer Granmo[✉]

Abstract—We present an all-digital programmable machine learning accelerator chip for image classification, underpinning on the Tsetlin machine (TM) principles. The TM is an emerging machine learning algorithm founded on propositional logic, utilizing sub-pattern recognition expressions called clauses. The accelerator implements the coalesced TM version with convolution, and classifies booleanized images of 28×28 pixels with 10 categories. A configuration with 128 clauses is used in a highly parallel architecture. Fast clause evaluation is achieved by keeping all clause weights and Tsetlin automata (TA) action signals in registers. The chip is implemented in a 65 nm low-leakage CMOS technology, and occupies an active area of 2.7 mm^2 . At a clock frequency of 27.8 MHz, the accelerator achieves 60.3k classifications per second, and consumes 8.6 nJ per classification. This demonstrates the energy-efficiency of the TM, which was the main motivation for developing this chip. The latency for classifying a single image is $25.4 \mu\text{s}$ which includes system timing overhead. The accelerator achieves 97.42%, 84.54% and 82.55% test accuracies for the datasets MNIST, Fashion-MNIST and Kuzushiji-MNIST, respectively, matching the TM software models.

Index Terms—Tsetlin machine, Accelerator, Machine learning, Image classification.

I. INTRODUCTION

HARDWARE (HW) accelerators are commonly integrated in modern electronic systems to relieve the burden on system processors from extensive application-specific workloads. Performance and energy-efficiency within a smaller form factor are key considerations for accelerator designs, particularly for Internet-of-Things (IoT), where the compute and memory resources of edge nodes typically are limited. In addition, such nodes are often battery-operated, and it is critical to minimize the overall energy footprints for longer battery operational lifetime.

Image classification is a key machine learning (ML) application, with usage scenarios across a wide range of IoT applications [1], such as industrial machine-vision, agricultural monitoring, unmanned aerial vehicles, room occupancy detection for building control systems, attention detection and gesture recognition.

Current methods for accelerating image classification in embedded systems, are predominantly based on convolutional neural networks (CNNs) [2], [3]. CNNs comprise many layers of multiply-and-accumulate (MAC) operations, each with their associated memory resources. As such, they require large number of micro-architectural operations for each classification

and have significant energy footprints [3]. The complexity and energy consumption can be reduced by compromising the data precision [4]. Binary and ternary activations and weights have been applied in several integrated circuit (IC) solutions that have shown good test accuracy with very low power consumption [5]–[9].

Unlike the numerical models based on neural networks mentioned above, the Tsetlin machine [10] is an ML algorithm founded on propositional logic. Parallel conjunctive clauses are defined by independent learning automata, and each clause represents a logical sub-pattern. The TM features a single-layer structure with highly interpretable outputs, making it well-suited for application areas such as biomedical, cybernetics, IoT, and law. Furthermore, because its primary operations are of Boolean type, TM solutions are hardware-efficient. The generation of a TM's output relies on summing and comparing class sums, with minimal or no need for energy-intensive multiplication operations, even during training. This makes TMs ideal for low-energy application-specific integrated circuit (ASIC) implementations [11]. Additionally, due to their small resource footprint, TMs facilitate hardware solutions that support on-device training and continuous learning [12].

The original TM version [10] is called the *vanilla TM*. For image classification, improved test accuracy is achieved by the *convolutional TM (CTM)* [13]. The CTM achieved a peak test accuracy of 99.4% on the MNIST dataset [14]. For the Fashion-MNIST (FMNIST) [15] and Kuzushiji-MNIST (KMNIST) [16] datasets, the peak test accuracies achieved were 91.5% and 96.31% respectively. Ensemble TM approaches have shown promising accuracies for more complex image datasets, such as CIFAR-10 and CIFAR-100, which are currently being investigated. In the case of CIFAR-10, the approach denoted *TM Composites* [17] has demonstrated a test accuracy of 82.8% [18].

In this paper, we present an inference accelerator ASIC based on the *coalesced TM (CoTM)* [19]. The CoTM utilizes a single clause pool, in contrast to the vanilla TM which uses one clause pool per class. As we operate the CoTM with convolution, we here denote it as a *convolutional CoTM (ConvCoTM)*. For configurations with few clauses, the ConvCoTM achieves better accuracy than the vanilla CTM, making it attractive for resource-constrained solutions.

Until now, only a single ASIC based on the TM has been reported [11], which operated on a simple dataset. We wanted

to make an accelerator that operated on a well-known dataset (MNIST) and to demonstrate that an all-digital TM-based ASIC could achieve energy-efficiency at the same level as analog in-memory-computing (IMC) solutions [9], [20], [21].

The ASIC's accelerator core is built on a modified version of the ConvCoTM inference core included in the FPGA solution in [12], which supported full on-device training. However, because of the FPGA it could not achieve ultra-low-power (ULP) operation. Compared to [12], several enhancements are made in the inference core of the ASIC, as described in section IV. In particular, there is an updated clause logic circuit with a novel feedback that reduces switching activity. There is also new functionality for loading a pre-trained model. Most important is the optimization of the inference part to achieve ULP operation.

Although MNIST is a simple dataset, it is still widely used for benchmarking of ULP image classification ASICs [9], [20], [21]. We therefore consider the MNIST dataset suitable for demonstrating the HW-friendliness and power-efficiency of a ConvCoTM-based accelerator, which was the main motivation for the design and implementation of this ASIC. The *main contributions* of our paper are:

- The accelerator is the first reported manufactured ASIC based on the CoTM. It is also the first TM ASIC where convolution is utilized.
- The accelerator is a fully digital, synchronous design, compatible with standard digital workflows. It operates with an energy per classification (EPC) of 8.6 nJ, which is the lowest reported for a fully digital solution running on the same dataset and with comparable test accuracy. Overall, it ranks as the second most energy-efficient solution. Other comparable solutions are of analog and mixed-signal type, utilizing IMC [9], [20], [21].
- The accelerator has low latency, essential for real-time operation in low-power systems with strict requirements.
- For TMs operating with convolution, we introduce a novel clause logic circuit with feedback, which reduces switching of the clause's combinational output.
- We describe an envisaged scaled-up ASIC that operates on the CIFAR-10 dataset, and provide estimates of its performance.

The remainder of the paper is organized as follows: Section II summarizes related work. Section III covers TM and CoTM background, including convolution operation. Section IV details the ASIC's architecture and building blocks. Measurement results are presented in Section V, followed by a discussion in Section VI before we conclude the paper.

II. RELATED WORK

In this section, we describe state-of-the-art works on low-power inference accelerators for image classification, as well as some reported TM-based HW solutions.

For low-power neural networks, digital Binary Neural Networks (BNNs) are widely utilized. A BNN-based accelerator IC module is detailed in [22]. This module was later included in a complete system-on-chip (SoC) [6]. When operating on

the CIFAR-10 [23] dataset, the SoC achieves 15.4 inferences/s and has a peak power envelope of 674 μ W. A 22 nm fully depleted silicon on insulator (FD-SOI) technology was used for the IC implementation.

In [7] a digital 10 nm FinFET CMOS solution is reported. Utilizing a BNN algorithm, it achieves a peak energy efficiency of 617 TOPS/W (Tera operations per second per watt). It has a power consumption of 5.6 mW and obtains an accuracy of 86% when operating on the CIFAR-10 dataset.

IMC solutions can provide very high energy-efficiency, as the bottleneck related to memory access is relieved. IMC has especially been utilized for analog/mixed-signal ML accelerator designs. An IMC mixed-signal 28 nm CMOS BNN processor is described in [5]. This accelerator achieves an EPC of 3.8 μ J when operating on CIFAR-10. The classification rate is 237 frames per second (FPS) with a power consumption of 0.9 mW.

In [9] a charge-domain IMC ternary neural network (TNN) chip is described. The main advantage of the ternary approach is a reduction of the required operations per classification with $3.9\times$ compared to a BNN model. The accelerator classifies MNIST images at a rate of 549 FPS, consuming 96 μ W. This corresponds to an EPC of 0.18 μ J. The test accuracy achieved is 97.1%.

The accelerator chip that achieves the lowest reported EPC for MNIST classification, is reported in [20]. It is a CNN utilizing an analog IMC architecture with time domain signal processing. It is implemented in 28nm CMOS and achieves an EPC of only 3.32 nJ.

Neuromorphic approaches, utilizing spiking neural networks (SNNs) have achieved very low energy consumption. In [21] a mixed-signal neuromorphic SNN IC is reported, which has been manufactured in a 65 nm CMOS technology. It achieves a test accuracy on MNIST of 95.35%, with a power consumption of 0.517 mW and an EPC of 12.92 nJ. Simulation results of a 28 nm CMOS charge-domain computing SNN solution are reported in [24]. The accelerator achieves an EPC of 15.09 nJ, a latency of 0.46 μ s and a test accuracy on MNIST of 94.81%. In [25], simulation results of a clock-free, event-driven, mixed-signal 28 nm IMC SNN are described. On MNIST it achieves a test accuracy of 96.92% and 1.38 nJ EPC.

For TM-based HW solutions, the first reported ASIC is described in [11]. It utilizes the vanilla TM architecture and operates on a 3-class machine learning (ML) problem. The chip is implemented in a 65 nm CMOS technology and supports both training and inference. In [26], the first TM-based HW accelerator with convolution is reported. It is an FPGA solution which operates on a 2-class pattern recognition problem (two-dimensional noisy XOR [13]) in 4×4 Boolean images, and employs a 2×2 convolution window. Full on-device training is implemented.

The FPGA solution in [27] is based on the vanilla TM and utilizes the sparsity of typical TM models, in combination with sequential operation. It represents a highly compact solution when it comes to HW resource usage.

In [12] the first reported ConvCoTM-based HW solution is presented, of which the inference part is the basis for our ASIC

as described in the Introduction section. It is an FPGA solution that classifies 28×28 images with 10 categories, and includes full on-device training. For the MNIST dataset a test accuracy of 97.6% is achieved, with a classification rate of 134k samples per second, and an EPC of $13.3 \mu\text{J}$. The source code for this design is available at [28].

In [29]–[31] the design and simulation of low-latency asynchronous TM solutions for inference and training are presented. A mixed-signal IMC TM solution is described in [32] with a simulated EPC for MNIST of 13.9 nJ. It is an inference solution with a Boolean-to-current architecture, and resistive RAM (ReRAM) transistor cells are employed to eliminate the need for energy-hungry analog-to-digital and digital-to-analog conversions. Another IMC TM design concept based on Y-flash cells, is reported in [33].

III. TM AND CoTM BACKGROUND

The basic concepts of a vanilla TM [10] are described here, followed by a description of general CoTM inference [19]. Later, we explain how to apply convolution to the CoTM. As the emphasis in this paper is on *inference* solutions, we do not include details about CoTM/ConvCoTM training, except for a brief description of the Tsetlin automaton (TA), which is the core learning element in a TM. TM training is covered in detail in the original TM, CTM and CoTM references [10], [13], [19]. A compact description of ConvCoTM training can be found in [12].

A. General TM Concepts

The input feature vector to a TM consists of o propositional Boolean variables, $x_u \in \{0, 1\}^o$, where $u \in \{0, \dots, o-1\}$. A new input vector named the *literals*, L , is generated by appending the negated variables to the input, as shown in Eq. (1). Thus, there are in total $2o$ literals.

$$L = [l_0, l_1, \dots, l_{2o-1}] \\ = [x_0, \dots, x_{o-1}, \neg x_0, \dots, \neg x_{o-1}] \quad (1)$$

A TA of two-action type [34] will either *include* or *exclude* a literal in a conjunctive *clause*, depending on its state. One team of TAs is applied per clause, and the different TA actions are obtained during the training process, which involves feedback mechanisms to each TA [10]. For an inference-only solution, as reported in this paper, only the *TA action signals* from the trained model are needed, not the complete TAs.

In a TM, the number of clauses, n , is a user specified integer. The output of a single clause, c_j , where $j \in \{0, \dots, n-1\}$, is given by

$$c_j = \bigwedge_{k \in I_j} l_k, \quad (2)$$

where l_k is the literal with index k . k belongs to $I_j \subseteq \{0, \dots, 2o-1\}$, where I_j is the set of indices of the literals in clause j for which the corresponding TAs take the action *include*.

B. CoTM

A vanilla TM employs one clause pool per class, and the clauses of each TM are grouped in two: positive and negative. In contrast, a CoTM [19] applies a single clause pool, common for all m outputs/classes. Different sets of weights, $w_{i,j}$, are applied to the clause outputs, $\{c_0, \dots, c_{n-1}\}$, to generate the class sums:

$$v_i = \sum_{j=0}^{n-1} w_{i,j} c_j, \quad (3)$$

where $i \in \{0, \dots, m-1\}$ is the class index.

The clause weights in Eq. (3) can have both positive and negative polarity, and obtain their values during training. *No multiplications* are needed to implement Eq. (3), only additions, as a clause can output either 0 or 1. The predicted class, \hat{y} , is determined by the *argmax* operator, as given by Eq. (4).

$$\hat{y} = \operatorname{argmax}_i \{v_i\}, \quad i \in \{0, \dots, m-1\}. \quad (4)$$

C. CoTM and Convolution

It has been shown that applying convolution to the TM can improve the image classification test accuracy [13]. Convolution also reduces the number of features that need to be processed simultaneously, which in turn reduces model size and design complexity. However, the benefits of convolution come at the cost of increased processing time, due to the need to sequentially process the various patches of the input sample.

For image classification, the input data samples to a ConvCoTM, are a set of images, each of dimensions $X \times Y$, with Z channels. The different patches of the image are generated by applying a sliding window of size $W_X \times W_Y$, with Z channels. The convolution window will be evaluated $B = B_X \times B_Y$ times across the image, where $B_X = 1 + (X - W_X)/d_x$, $B_Y = 1 + (Y - W_Y)/d_y$, and d_x and d_y are the stride values of the convolution window in the X and Y directions respectively [13]. For each window position, the number of Boolean features generated per patch is given by

$$N_F = W_X \times W_Y \times Z \times U + (Y - W_Y) + (X - W_X). \quad (5)$$

In Eq. (5), U is the number of bits used for thermometer encoding [35] of the value of a single pixel (one-hot encoding can also be used). Such encoding is required because a TM operates on Boolean variables, not on binary numbers. The term $(Y - W_Y) + (X - W_X)$ in Eq. (5) represents the number of bits that encode the patch's position [12], [19] in the Y and X directions respectively. Also here we apply thermometer encoding. As shown in Eq. (1), the ConvCoTM also takes as input the negated versions of the features to form the *literals* per patch.

D. Datasets and Booleanization

The widely used MNIST [14] dataset consists of handwritten digits. FMNIST [15] is more challenging than MNIST and includes images from a Zalando catalog, such as t-shirts,

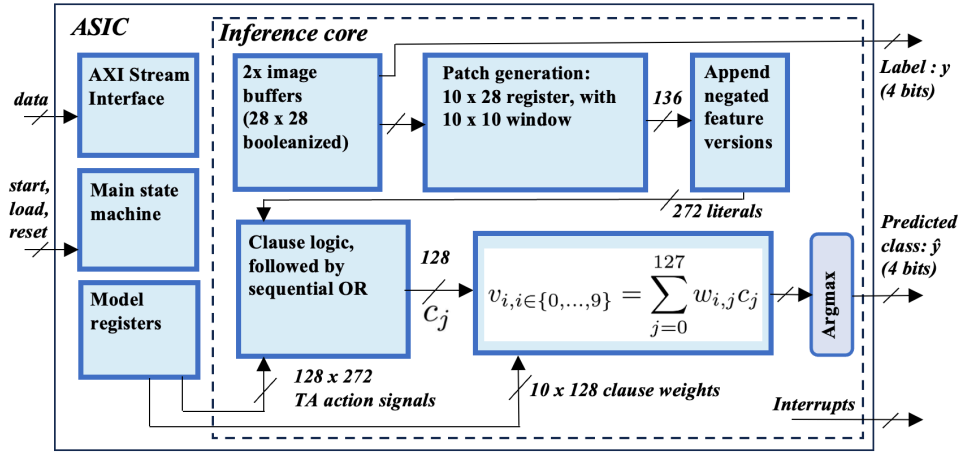


Fig. 1. ConvCoTM accelerator ASIC block diagram.

sandals, and shoes. KMNIST [16] consists of cursive Japanese characters, and is also more demanding than MNIST. Each of these datasets includes images of 28×28 pixels organized in 60k training samples and 10k test samples. There are 10 classes within each dataset. As the images are of single-channel (greyscale) type, $Z = 1$.

The pixel values range from 0 to 255. For MNIST, they are converted into Boolean variables (i.e., *booleanized*) with simple thresholding, where pixel values larger than 75 are replaced with 1, and 0 otherwise [13]. For FMNIST and KMNIST, an adaptive Gaussian thresholding procedure [13] is applied. We use one bit per pixel, i.e., $U = 1$ for all three datasets. The convolution window has dimensions $W_X = W_Y = 10$, and a step size of one is used in both directions. For each patch, we have 100 feature bits from the convolution window plus 36 bits for the appended patch position information, ref. Eq. (5). The number of literals for each patch is therefore 272.

E. TM and Convolution - Inference

During inference, each clause in a ConvCoTM is evaluated B times per image. After finishing the patch generation, a clause will output 1 if it has recognized a pattern *at least once* in any of the B patches for a given image [13]. The clause output is given by Eq. (6) which we call the *sequential OR-function*. Here c_j is the j 'th clause of the ConvCoTM, and c_j^b is the b 'th output of this clause obtained during the patch generation:

$$c_j = \bigvee_{b=0}^{B-1} c_j^b. \quad (6)$$

Class sum generation and class prediction are similar to the case without convolution, and follow Eq. (3) and Eq. (4).

IV. DESIGN OVERVIEW

The block diagram of the ConvCoTM accelerator is shown in Fig. 1. The accelerator includes all circuitry required for performing inference, and only minimal interaction with the system processor is required. The three main modules are i) a data interface for transfer of model parameters and

image samples, ii) a module for model storage and iii) an inference core that performs classification of an image. The following subsections describe the different sub-modules and the accelerator's operation in detail.

A. Interface to the System Processor

An external system processor is required for i) applying a few single-bit control signals to the accelerator, ii) feeding data to the accelerator and iii) reading interrupt signals and class predictions from the accelerator. All other operations are performed by the accelerator.

The 8-bit parallel data interface towards the external system processor, is inspired by the ARM AXI Stream interface [36]. It is used for transferring model data to the accelerator during *load model mode*, and for transferring images in *inference mode*. When a classification operation is finished, the accelerator outputs an interrupt. In addition, it outputs a separate 8-bit signal consisting of the predicted class of the sample together with the true label (if provided).

B. ConvCoTM Model Registers

The *model* of a given CoTM configuration consists of: i) the TA action signals (*include/exclude signals*) *per clause* and ii) the signed weights *per clause per class*. The TA action signals are stored in registers, readily available for simultaneous clause evaluation. These signals require $272 \times 128 = 34816$ D flip-flops (DFFs). Registers are also applied for the clause weights per class. For this ASIC, eight bits are allocated per weight, with two's complement representation. The number of DFFs for storing the weights is $10 \times 128 \times 8 = 10240$, and the complete model size used by the accelerator is 45056 bits, i.e., 5632 bytes.

C. Image Data Buffer and Patch Generation

The accelerator includes a data buffer with room for two complete 28×28 booleanized images. While one image is being processed, another image can be transferred from the external system processor to the other image register, thereby improving throughput. We denote this as *continuous*

classification mode. The size of a complete booleanized image is $28 \times 28 / 8$ bytes = 98 bytes. One additional byte is allocated for the image label (0 to 9).

The patch generation module consists of a register with 10 rows, each with 28 DFFs. At the start of processing a new sample, the first 10 rows of an image are loaded into the register, and the convolution window starts at the leftmost position, which has coordinates (0, 0).

During the patch generation, the window is moved to the right with increments of one. As described in Subsection III-C, the position of the window is thermometer encoded. There are 19 different x -coordinates for the window, requiring 18 bits. When the window has been evaluated at the rightmost x -position (0, 18), the contents of all 10 rows are shifted upwards with one step, and the next image datarow is loaded into the lowermost register row. The convolution window then starts again at the leftmost position, now with patch coordinates (1, 0). This procedure is repeated until all 28 datarows of the image have been processed. There are 19 different positions also for the y -coordinate, and during a complete patch generation phase, $19 \times 19 = 361$ patches are generated.

D. Clause Pool

The ConvCoTM is configured with 128 clauses that operate in parallel. Each clause takes the literals, $[l_0, l_1, \dots, l_{271}]$, as input, as well as their corresponding TA action signals, $[i_{j,0}, i_{j,1}, \dots, i_{j,271}]$, $j \in \{0, \dots, 127\}$, from the model register. Fig. 2 shows a simplified circuit diagram of the clause logic. A literal will be included in the logical AND expression, that constitutes the *clause*, if its corresponding TA action signal is high. A special situation occurs when a clause is *empty*, i.e., when there are no *include* TA actions. In this case, additional logic will set the signal *Empty* high, forcing c_j^b low.

The DFF in Fig. 2 constitutes a single-bit register for clause j . Its content, c_j , is ORed with the combinational clause value, c_j^b , of the current patch, during the patch generation. This implements the *sequential OR function* in Eq. (6). The DFF is reset before starting a new convolution process.

The signal c_j is also fed back to the input of the OR-gates, as there is no need for the combinational logic to evaluate a clause for more patches if c_j already is high. This feedback, hereinafter denoted the *clause switching reduction feedback* (CSRF), reduces the switching in the combinational part of the clause logic. Simulations of MNIST classification utilizing CSRF, showed an average of 50% reduction in the toggling rate of c_j^b for each clause. The accelerator ASIC has a dedicated pin that can enable or disable the CSRF.

In this accelerator ASIC we apply a single convolution window. If increased classification rate is wanted, one can use several convolution windows that operate in parallel. In this case, the combinational clause logic that generates the signal c_j^b in Fig. 2, would have to be replicated for each convolution window.

E. Inference

The inference operation starts with loading an image into the data buffer, followed by sequential generation of the patches,

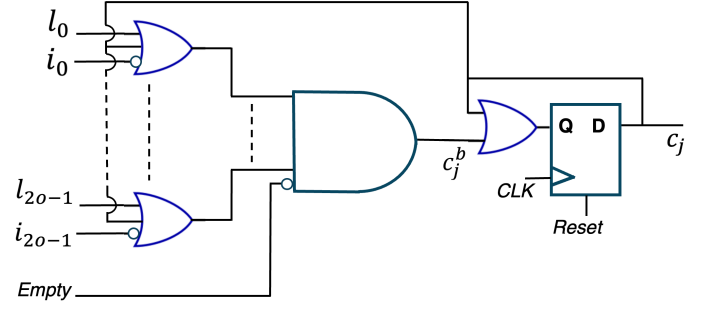


Fig. 2. Circuitry for a single clause. Literals are denoted with l and TA-actions with i .

as described in Subsection IV-C. When finished, each clause value, c_j , is weighted, for each class, according to Eq. (3).

All ten class sums are generated in parallel, by adders configured in a tree-structure and utilizing a three-stage pipeline. Finally, an *argmax* module [11] selects the class with the highest class sum, as the *predicted class*, \hat{y} . Fig. 3 shows a simplified state diagram of the accelerator.

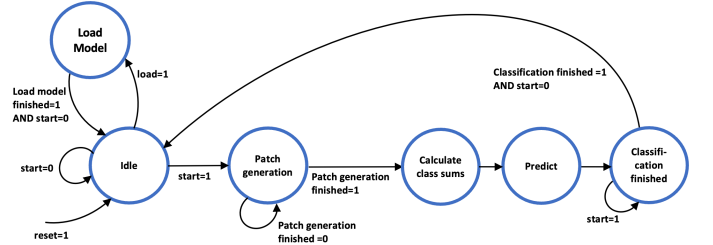


Fig. 3. Simplified accelerator state diagram.

The accelerator's latency is 471 clock cycles. This is measured from when the system processor initiates the first byte transfer of the image, until a prediction is available. It includes 99 clock cycles for transferring the 98 image bytes and the label byte, and 372 clock cycles for the patch generation, class summation and class prediction.

When the accelerator operates in continuous mode, a new sample is loaded into the image buffer while the current sample is being processed, see Subsection IV-C. This increases the throughput, as image samples can be processed every 372th clock cycle. Any timing overhead in the system processor will add to the total latency.

F. Clock Domains

The key to reducing the digital switching power of the accelerator, lies at the top level of the ASIC architecture. Two separate clock domains are utilized, each with its own dedicated clock pin, assigned to the model part and the inference core, respectively.

When a model has been transferred from the system processor to the ASIC, the TA action signals and the weights are available in registers that do not need further clocking. By stopping the clock to the model part, when operating in

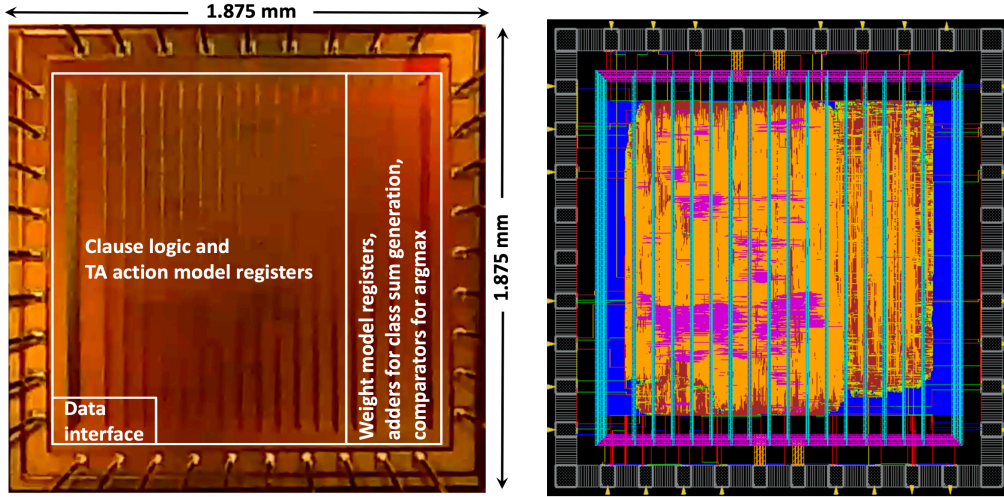


Fig. 4. Photo and layout plot of the ConvCoTM accelerator chip.

inference mode, the digital switching power is reduced significantly, as the model part constitutes approximately 90% of the accelerator's DFFs. To further reduce power consumption, standard clock gating is applied for the inference module. This ensures, for instance, that the pipelined registers associated with the class sum generation are enabled and clocked only for four clock cycles per classification phase. The clock-gating can be enabled/disabled by an external pin.

V. IMPLEMENTATION AND MEASUREMENT RESULTS

The ConvCoTM accelerator was designed in VHDL and implemented in a 65 nm low-leakage CMOS technology from UMC. A JLCC44 ceramic package housed the chip. Fig. 4 shows a photograph and a layout plot of the ASIC. The accelerator's core area is approximately 2.7 mm^2 . The VHDL source code for the ASIC implementation (used for initial FPGA verification) is available at a GitHub repository [37].

A printed circuit board (PCB) was developed for testing and characterization of the ASIC. The ASIC PCB was connected to a Digilent Zybo Z7-20 development board, equipped with a Xilinx Zynq XC7Z020 FPGA, as shown in Fig. 5. One of the FPGA's ARM9 cores was configured as system processor, and the FPGA board provided clocks, model data, image data samples and control signals to the ASIC PCB. The processor also read back accelerator status signals, and the predicted class per sample. To interface with the FPGA board, the ASIC's input/output (IO) ports operated at 3.3 V supply voltage. The accelerator core operated from 0.82 V to 1.2 V.

For each of the datasets MNIST, FMNIST and KMNIST, the *Tsetlin Machine Unified* (TMU) SW-version [38] of the ConvCoTM was trained to find suitable models. Maximum/minimum limits were set on the clause weights to fit with the allocated 8-bits per weight in the accelerator. For simplicity, the images from the test datasets were preprocessed (booleanized), as described in Subsection III-D, and included in the FPGA processor's test program.

Model data and image samples were applied from the FPGA to the accelerator via the AXI Stream interface. We

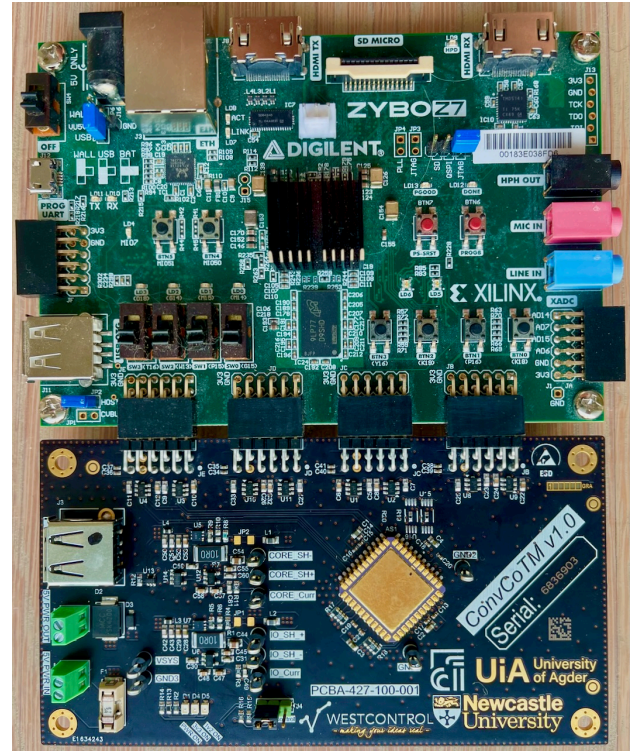


Fig. 5. Test setup with the ConvCoTM ASIC test board connected to the FPGA development board.

utilized direct memory access (DMA) functionality on the FPGA to enable fast data transfer. The maximum classification rate achieved, including system processor timing overhead, was 60.3k images per second in continuous mode, with an accelerator clock frequency of 27.8MHz. The maximum operating frequency was limited by the general purpose IOs (GPIOs) on the FPGA board. When classifying a single image, the latency was $25.4 \mu\text{s}$, including the transfer time of the image to the accelerator as well as timing overhead in the system processor.

The achieved test accuracies of the datasets MNIST,

TABLE I
THE CONVCoTM ACCELERATOR ASIC'S MAIN CHARACTERISTICS AND PERFORMANCE

Parameter / Characteristics	Value / Description
Technology	65 nm low-leakage CMOS from UMC
Chip area (full die)	3.5 mm ²
Chip area (core)	2.7 mm ²
Gatecount (core)	201k cells including 52k DFFs
Power consumption (accelerator core only)	1.15 mW ^{a,c} 0.52 mW ^{a,d} 81 μ W ^{b,c} 21 μ W ^{b,d}
Classification rate (including system overhead)	60.3k images/s ^a 2.27k images/s ^b
Energy per classification (accelerator core only)	19.1 nJ ^{a,c} 8.6 nJ ^{a,d} 35.3 nJ ^{b,c} 9.6 nJ ^{b,d}
Latency (single image classification including data transfer)	25.4 μ s ^a 0.66 ms ^b
Test accuracy	97.42% (MNIST) 84.54% (FMNIST) 82.55% (KMNIST)

^a 27.8 MHz clock frequency. ^b 1.0 MHz clock frequency. ^c The accelerator core supply voltage (vdd) is 1.20 V. ^d vdd=0.82 V.

FMNIST and KMNIST were 97.42%, 84.54% and 82.55% respectively. These results are independent of the accelerator clock frequency and are exactly in accordance with the performance of the models obtained from the SW simulations.

For power consumption measurements, a Joulescope JS220 precision energy analyzer was used. The power consumption during inference was measured while the accelerator was set in a test mode with repeated classifications of the full 10k sample dataset. The power consumed by the accelerator core with 1.20 V supply voltage and a clock frequency of 27.8 MHz was 1.15 mW. This corresponds to an EPC of 19.1 nJ. With a supply voltage of 0.82 V, the accelerator core's power consumption was 0.52 mW and the corresponding EPC was 8.6 nJ. With 1.2 V core supply voltage and a clock frequency of 1 MHz, the achieved classification rate was 2.27k FPS at a power consumption of 81 μ W.

Table I summarizes the characteristics and performance of the accelerator. In a real application, the ConvCoTM design would typically be included as a peripheral module to a microcontroller in an SoC. Therefore, we considered the power consumption of the accelerator *core* as the most interesting power parameter. In inference mode, the digital 3.3 V IOs, which were required for interfacing to the FPGA board, had a power consumption of 0.76 mW, at a clock frequency of 27.8 MHz.

All power and energy measurement results of the ASIC are average values, and were performed with clock-gating and CSRF enabled (as shown in Fig. 2). When operating at 27.8 MHz, clock-gating reduced the power consumption by approximately 60%, while the CSRF alone provided less than 1% power reduction.

VI. DISCUSSIONS

We consider the ConvCoTM accelerator with 128 clauses as a small configuration. In light of this, we are satisfied with the obtained test accuracy which is comparable with other low-complexity and ULP solutions. Table II shows the performance and properties of state-of-the-art ULP IC implementations for classification of MNIST and CIFAR-10 datasets. Inspired by the *TinyML* [39] benchmarks for embedded systems, we specify the *classification rate*, the *peak power consumption* and the *EPC*. These are system parameters which are independent of the accelerator model and architecture [40]. However, when used for comparing solutions, one must be careful to specify the ML task performed. The CIFAR-10 dataset is significantly more challenging than MNIST. Therefore, accelerators that operate on CIFAR-10, have lower classification rates and higher EPC compared to accelerators that operate on MNIST.

The mixed-signal IMC-based solution in [9] operates with a peak power consumption of 96 μ W and consumes 0.18 μ J per classification on MNIST, with a test accuracy of 97.1%. In [21] a mixed-signal SNN IC accelerator achieves an EPC of 12.92 nJ with 0.7 V supply voltage. It utilizes a time-domain echo state network (ESN) [41] approach and thus requires non-standard interfacing with the surrounding system's resources. The test accuracy achieved on MNIST is 95.35%. The 28 nm CMOS CNN-based accelerator in [20] utilizes an IMC architecture with analog and time-domain signal processing. It achieves an EPC of 3.32 nJ, which is the lowest reported for MNIST.

Our ConvCoTM accelerator ASIC achieves an EPC of 8.6 nJ at 0.82 V operating voltage. This is the second lowest EPC reported, for a manufactured ASIC that operates on MNIST. As the ConvCoTM ASIC is fully digital, the classification rate and thereby also the peak power consumption, can be scaled by adjusting the clock frequency. At a clock frequency of 1 MHz, the power consumption is 81 μ W.

Most ULP accelerators are based on analog techniques [5], [9], [20], [21]. The test accuracy of such solutions is susceptible to variations in process parameters, supply voltage and operating temperature (PVT). All-digital solutions, like our ConvCoTM ASIC and [6]–[8], avoid such non-ideal effects. In addition, these accelerators are easier to integrate in larger SoCs, and can more easily be scaled and re-targeted to other technologies. This applies for CNNs as well as TMs.

In the ConvCoTM accelerator, the combinational clause logic draws only a small amount of energy compared to the clock tree of the inference-core DFFs. This is the main reason why the CSRF technique (see Subsection IV-D) did not provide a greater reduction in EPC. Other convolutional TM architectures, that operate at higher clock frequencies, process more literals in parallel, and utilize sparsity in TM models, can potentially benefit more from the CSRF technique.

VII. SCALING

The ConvCoTM accelerator's architecture described in this paper, is highly suited for scaling, and can be modified to operate on larger and more complex images. There is active research on how to apply the TM algorithm for larger and

TABLE II
COMPARISON OF THE CONVCoTM IC ACCELERATOR WITH PREVIOUS WORKS.

	This work	TCAS-I'25 Zhao [20]	TCAS-II'23 Yejun [21]	JSSC'23 Yang [9]	TCAS-I'20 Mauro [6]	JSSC'21 Knag [7]	TCAS-I'20 Bankman [5]
Technology	65 nm CMOS	28 nm CMOS	65 nm CMOS	40 nm CMOS	22 nm FD-SOI	10 nm FinFET	28 nm CMOS
Active area	2.7 mm ²	0.261 mm ²	0.57 mm ²	0.98 mm ²	2.3 mm ²	0.39 mm ²	4.6 mm ²
Algorithm	ConvCoTM	CNN	SNN	Ternary CNN	BNN	BNN	BNN
Design type	Digital	Analog, time domain	Neuromorphic mixed-signal	IMC, mixed-signal	Digital (SoC)	Digital	IMC, mixed-signal
Image dataset	MNIST, FMNIST, KMNIST	MNIST	MNIST	MNIST	CIFAR-10	CIFAR-10	CIFAR-10
Measured test accuracy	97.42%, 84.54%, 82.55%	97.9%	95.35%	97.1%	99% of nominal accuracy	86%	86%
Classifications per second	60.3k ^a 2.27k ^b	3508	233k (1.2 V) 40k (0.7 V)	549	15.4	Not stated	237
Latency ^c	25.4 μ s ^a 0.66 ms ^b	Not stated	Not stated	Not stated	Not stated	Not stated	Not stated
Inference power	1.15 mW ^{a,c} 0.52 mW ^{a,d} 81 μ W ^{b,c} 21 μ W ^{b,d}	11.6 μ W	9.37 mW (1.2 V) 0.517 mW (0.7 V)	96 μ W	674 μ W ^f	5.6 mW (13 MHz) 607 mW (622 MHz)	0.9 mW
Energy per classification (EPC)	19.1 nJ ^{a,c} 8.6 nJ ^{a,d} 35.3 nJ ^{b,c} 9.6 nJ ^{b,d}	3.32 nJ	40.17 nJ (1.2 V) 12.92 nJ (0.7 V)	0.18 μ J	43.8 μ J	Not stated	3.8 μ J

^a 27.8 MHz clock frequency. ^b 1.0 MHz clock frequency. ^c The accelerator core supply voltage (vdd) is 1.20 V. ^d vdd=0.82 V. ^e For processing of a single image sample, including data transfer. ^f Full SoC.

more complex images. The TM version that currently achieves the best test accuracy on CIFAR-10 is *TM Composites* [17], [18]. Here, several *TM Specialists* are applied to an image sample. Examples of *specializations* are different booleanization techniques and convolution window sizes. After an image has been processed, the class sums from each TM Specialist are normalized, followed by summation per class. Finally, an *argmax* operator is applied on the *composite class sums* for output prediction.

Table III shows characteristics and performance estimates for an envisaged TM Composites ASIC design, intended for inference operation on CIFAR-10 images. It is assumed that one configurable TM module is implemented in the ASIC, and models for four different TM Specialist configurations are applied in sequence, through transferring a new model from on-chip ultra-low-power RAM per configuration.

Booleanization of the images, for the different TM Specialists, is assumed to be performed by dedicated logic in the HW accelerator. We assume a timing-optimized data interface, with line buffers [42], allowing the patch generation to start as soon as a sufficient number of image lines have been transferred to the accelerator.

For the TM Specialists, we assume an average number of literals per patch of 1000, and by utilizing the technique described in [43], the number of literals is limited to 16 per clause. For the TA actions, the model for each TM Specialist therefore needs to include 16 ten-bit literal addresses per clause.

We assume the same 65 nm CMOS technology is used as for the current ConvCoTM ASIC. The chip area for the CIFAR-10 accelerator is estimated by multiplying the chip area of the current ASIC (2.7 mm²) with the ratio, R , given by the model size of one TM Specialist (32.5 kilobyte) divided by the model size of the ASIC in this paper (5.6 kilobyte). We therefore get $R = 32.5/5.6 \approx 5.8$. This is a reasonable assumption because

the model storage in registers (for the active TM Specialist) and the clause logic, dominate the chip area. We further assume 2 mm² in additional chip area for booleanization logic, additional adders for class sum generation, and RAM modules for model storage.

We estimate that each TM Specialist will need approximately 1000 clock cycles for the processing per sample, including booleanization. In addition, before a TM Specialist can start operating, its model has to be loaded from on-chip RAM. We assume the model is organized in memory such that a transfer rate of 32 bytes per clock cycle is enabled. Thus, we will need approximately 1020 clock cycles for a complete model transfer. A single TM Specialist will therefore require in total about 2020 clock cycles to process a sample, and with four TM Specialists we will need approximately 8080 clock cycles for a complete classification. With a system clock of 27.8 MHz (as for the current ConvCoTM ASIC), the classification rate would be $27.8 \times 10^6 / 8080 \text{ FPS} \approx 3440 \text{ FPS}$.

An estimate of the power consumption is found by multiplying the power consumption of the current ASIC's accelerator core, operating at 27.8 MHz (1.15 mW), with the factor R . During model loading and booleanization, we assume power consumption similar to that during inference. An estimate of the energy per classification is then $R \times 1.15 \text{ mW} / (3440 \text{ FPS}) \approx 1.9 \mu\text{J/frame}$.

VIII. CONCLUSION

In this work, an ASIC implementation of a ConvCoTM accelerator for inference is presented. It operates on booleanized images of 28×28 pixels, and samples are classified into 10 categories. A pool of 128 clauses, i.e., pattern recognition logical expressions, is applied for the accelerator. The solution is fully programmable, and achieves a test accuracy of 97.42% on MNIST. With a clock frequency of 27.8 MHz, the accelerator's throughput is 60.3k images per second, and with

TABLE III
ENVISAGED CONVCoTM INFERENCE ASIC CONFIGURATION AND
PERFORMANCE FOR OPERATION ON THE CIFAR-10 DATASET, BASED ON
THE TM COMPOSITES ARCHITECTURE.

Parameter	Value	Comment
Number of TM specialists	4	4 × 4 color thermometer, 3 × 3 color thermometer, 32 × 32 histogram of gradients, 10 × 10 adaptive thresholding.
Number of clauses	1000	
Number of included literals per clause	16	We assume 1000 literals per patch, and literal limitation based on [43].
Model size: TA actions per TM Specialist	20 kilobyte	1000 clauses, each with 16 literals. The address length per literal is 10 bits.
Model size: Weights per TM Specialist	12.5k kilobyte	10 classes, 1000 clauses and 10-bit weights.
Complete model size	130 kilobyte	For four TM Specialists.
Classification rate	3440 FPS	Sequential operation of the TM Specialists, 27.8 MHz system clock, complete model stored on-chip, without system processor overhead.
Test accuracy	79%	Estimate for CIFAR-10.
Accelerator core	17.7 mm ²	65 nm CMOS.
Accelerator core power consumption	6.7 mW	Inference mode, 27.8 MHz system clock.
Accelerator core energy per classification.	1.9 μJ	Inference mode, 27.8 MHz system clock.

an operating voltage of 0.82 V, the energy consumed by the accelerator core per classification is 8.6 nJ. We believe the TM represents an attractive ML solution for low-power edge nodes in IoT systems for various workloads. The ASIC demonstrates the simplicity, hardware-friendliness and power-efficiency of all-digital TM solutions.

ACKNOWLEDGMENTS

The authors would like to thank Adrian Wheeldon (Literal Labs, UK) and Jordan Morris (UK) for valuable general ASIC implementation discussions. Thank you also to Joel Trickey (STFC, UK) for support with IC design backend tools, and to Alberto Pagotto (imec.IC-Link, Belgium) for help during the ASIC tapeout phase. Finally, we would like to thank Geir Rune Angell (Westcontrol, Norway) for the design of the ASIC test board.

REFERENCES

- [1] M. Maheepala, M. A. Joordens, and A. Z. Kouzani, "Low power processors and image sensors for vision-based IoT devices: A review," *IEEE Sensors Journal*, vol. 21, no. 2, pp. 1172–1186, 2020.
- [2] Y. LeCun, "Deep learning hardware: Past, present, and future," in *2019 IEEE International Solid-State Circuits Conference - (ISSCC)*, 2019, pp. 12–19.
- [3] V. Sze, Y.-H. Chen, T.-J. Yang, and J. S. Emer, "Efficient processing of deep neural networks: A tutorial and survey," *Proceedings of the IEEE*, vol. 105, no. 12, pp. 2295–2329, 2017.
- [4] J. Dean, "The deep learning revolution and its implications for computer architecture and chip design," in *IEEE ISSCC*, 2020, pp. 8–14.
- [5] D. Bankman, L. Yang, B. Moons, M. Verhelst, and B. Murmann, "An always-on 3.8 μJ/86% CIFAR-10 mixed-signal binary CNN processor with all memory on chip in 28-nm CMOS," *IEEE JSSC*, vol. 54, pp. 158–172, 1 2019.

- [6] A. D. Mauro, F. Conti, P. D. Schiavone, D. Rossi, and L. Benini, "Always-on 674μW@4GOP/s error resilient binary neural networks with aggressive SRAM voltage scaling on a 22-nm IoT end-node," *IEEE TCAS-I*, vol. 67, no. 11, pp. 3905–3918, 2020.
- [7] P. C. Knag, G. K. Chen, H. E. Sumbul, R. Kumar, S. K. Hsu, A. Agarwal, M. Kar, S. Kim, M. A. Anders, H. Kaul, and R. K. Krishnamurthy, "A 617-TOPS/W all-digital binary neural network accelerator in 10-nm FinFET CMOS," *IEEE JSSC*, vol. 56, no. 4, pp. 1082–1092, 2021.
- [8] R. Andri, L. Cavigelli, D. Rossi, and L. Benini, "YodaNN: An architecture for ultralow power binary-weight CNN acceleration," *IEEE TCAD*, vol. 37, pp. 48–60, 1 2018.
- [9] X. Yang, K. Zhu, X. Tang, M. Wang, M. Zhan, N. Lu, J. P. Kulkarni, D. Z. Pan, Y. Liu, and N. Sun, "An in-memory-computing charge-domain ternary CNN classifier," *IEEE JSSC*, vol. 58, no. 5, pp. 1450–1461, 2023.
- [10] O.-C. Granmo, "The Tsetlin machine – A game theoretic bandit driven approach to optimal pattern recognition with propositional logic," *arXiv e-prints*, 2018. [Online]. Available: <https://arxiv.org/abs/1804.01508>
- [11] A. Wheeldon, R. Shafik, T. Rahman, J. Lei, A. Yakovlev, and O.-C. Granmo, "Learning automata based energy-efficient AI hardware design for IoT applications," *Philosophical Transactions of the Royal Society A: Mathematical, Physical and Engineering Sciences*, vol. 378, no. 2182, 2020.
- [12] S. A. Tunheim, L. Jiao, R. Shafik, A. Yakovlev, and O.-C. Granmo, "Tsetlin machine-based image classification FPGA accelerator with on-device training," *IEEE Transactions on Circuits and Systems I: Regular Papers*, vol. 72, no. 2, pp. 830–843, 2025.
- [13] O.-C. Granmo, S. Glimsdal, L. Jiao, M. Goodwin, C. W. Omlin, and G. T. Berge, "The convolutional Tsetlin machine," *arXiv e-prints*, 2019. [Online]. Available: <https://arxiv.org/abs/1905.09688>
- [14] Y. LeCun and C. Cortes, "MNIST handwritten digit database," 2010. [Online]. Available: <http://yann.lecun.com/exdb/mnist/>
- [15] Fashion-MNIST Repo., <https://www.openml.org/search?type=data&status=active&id=40996&sort=runs>, 2017.
- [16] Kuzushiji-MNIST Repo., <https://github.com/rois-codh/kmnist?tab=readme-ov-file>, 2019.
- [17] O.-C. Granmo, "TMComposites: Plug-and-play collaboration between specialized Tsetlin machines," 2023. [Online]. Available: <https://arxiv.org/pdf/2309.04801.pdf>
- [18] Y. Grønningsæter, H. S. Smørvik, and O.-C. Granmo, "An optimized toolbox for advanced image processing with Tsetlin machine composites," *arXiv e-prints*, 2024.
- [19] S. Glimsdal and O.-C. Granmo, "Coalesced multi-output Tsetlin machines with clause sharing," *arXiv e-prints*, 2021. [Online]. Available: <https://arxiv.org/abs/2108.07594>
- [20] Y. Zhao, P. He, Y. Zhu, R. P. Martins, C.-H. Chan, and M. Zhang, "A 28-nm 3.32-nJ/frame compute-in-memory CNN processor with layer fusion for always-on applications," *IEEE Transactions on Circuits and Systems I: Regular Papers*, pp. 1–13, 2025.
- [21] Y. Ko, S. Kim, K. Shin, Y. Park, S. Kim, and D. Jeon, "A 65 nm 12.92-nJ/inference mixed-signal neuromorphic processor for image classification," *IEEE Transactions on Circuits and Systems II: Express Briefs*, vol. 70, no. 8, pp. 2804–2808, 2023.
- [22] F. Conti, P. Schiavone, and L. Benini, "XNOR neural engine: A hardware accelerator IP for 21.6 fJ/op binary neural network inference," *IEEE TCAD*, vol. 37, pp. 2940–2951, 11 2018.
- [23] A. Krizhevsky, "Learning multiple layers of features from tiny images," <https://www.cs.toronto.edu/~kriz/cifar.html>, 2009.
- [24] Y. Zhang, Z. Xuan, and Y. Kang, "A 28nm 15.09nJ/inference neuromorphic processor with SRAM-based charge domain in-memory-computing," in *2023 IEEE 15th International Conference on ASIC (ASICON)*, 2023, pp. 1–4.
- [25] W. Fang, Z. Xuan, S. Chen, and Y. Kang, "An 1.38nJ/inference clock-free mixed-signal neuromorphic architecture using ReL-PSP function and computing-in-memory," in *2023 IEEE Biomedical Circuits and Systems Conference (BioCAS)*, 2023, pp. 1–5.
- [26] S. A. Tunheim, L. Jiao, R. Shafik, A. Yakovlev, and O.-C. Granmo, "Convolutional Tsetlin machine-based training and inference accelerator for 2-D pattern classification," *Microprocessors and Microsystems*, vol. 103, p. 104949, 2023.
- [27] P. K. Sahu, S. Boppu, R. Shafik, S. A. Tunheim, O.-C. Granmo, and L. R. Kennermaddi, "Enhancing inference performance through include only literal incorporation in Tsetlin machine," in *2023 International Symposium on the Tsetlin Machine (ISTM)*, 2023, pp. 1–8.
- [28] GitHub repository for a ConvCoTM FPGA solution with on-device training, <https://github.com/satunheim/ConvCoTM-FPGA-28x28>.

- [29] A. Wheeldon, A. Yakovlev, R. Shafik, and J. Morris, "Low-latency asynchronous logic design for inference at the edge," in *2021 Design, Automation & Test in Europe Conference & Exhibition (DATE)*, 2021, pp. 370–373.
- [30] A. Wheeldon, A. Yakovlev, and R. Shafik, "Self-timed reinforcement learning using Tsetlin machine," in *2021 27th IEEE International Symposium on Asynchronous Circuits and Systems (ASYNC)*, 2021, pp. 40–47.
- [31] T. Lan, O. Ghazal, S. Ojukwu, K. Krishnamurthy, R. Shafik, and A. Yakovlev, "An asynchronous winner-takes-all arbitration architecture for Tsetlin machine acceleration," in *2024 22nd IEEE Interregional NEWCAS Conference (NEWCAS)*, 2024, pp. 16–20.
- [32] O. Ghazal, S. Singh, T. Rahman, S. Yu, Y. Zheng, D. Balsamo, S. Patkar, F. Merchant, F. Xia, A. Yakovlev *et al.*, "IMBUE: In-memory boolean-to-current inference architecture for Tsetlin machines," in *2023 IEEE/ACM International Symposium on Low Power Electronics and Design (ISLPED)*. IEEE, 2023, pp. 1–6.
- [33] O. Ghazal, T. Lan, S. Ojukwu, K. Krishnamurthy, A. Yakovlev, and R. Shafik, "In-memory learning automata architecture using Y-flash cell," 2024. [Online]. Available: <https://arxiv.org/abs/2408.09456>
- [34] M. L. Tsetlin, "On behaviour of finite automata in random medium." *Avtomat. i Telemekh*, 22(10), pp. 1345–1354, 1961.
- [35] J. Buckman, A. Roy, C. Raffel, and I. Goodfellow, "Thermometer encoding: One hot way to resist adversarial examples," in *ICLR*, 2018.
- [36] AMBA AXI4 interface protocol, <https://www.xilinx.com/products/intellectual-property/axi.html>.
- [37] GitHub repository for a ConvCoTM inference ASIC, https://github.com/satunheim/ConvCoTM_Inference_Accelerator.
- [38] Tsetlin machine unified (TMU) CoTM github repository, https://github.com/cair/tmu/blob/main/tmu/models/classification/coalesced_classifier.py, 2023.
- [39] C. Banbury, V. J. Reddi, P. Torelli, J. Holleman, N. Jeffries, C. Kiraly, P. Montino, D. Kanter, S. Ahmed, D. Pau, U. Thakker, A. Torrini, P. Warden, J. Cordaro, G. D. Guglielmo, J. Duarte, S. Gibellini, V. Parekh, H. Tran, N. Tran, N. Wenxu, and X. Xuesong, "MLPerf tiny benchmark," *arXiv e-prints*, 2021. [Online]. Available: <https://arxiv.org/abs/1905.09688>
- [40] V. Sze, Y.-H. Chen, T.-J. Yang, and J. S. Emer, "How to evaluate deep neural network processors: TOPS/W (alone) considered harmful," *IEEE Solid-State Circuits Magazine*, vol. 12, no. 3, pp. 28–41, 2020.
- [41] M. Lukoševičius and H. Jaeger, "Reservoir computing approaches to recurrent neural network training," *Computer Science Review*, vol. 3, no. 3, pp. 127–149, 2009. [Online]. Available: <https://www.sciencedirect.com/science/article/pii/S1574013709000173>
- [42] H. Wang, T. Wang, L. Liu, H. Sun, and N. Zheng, "Efficient compression-based line buffer design for image/video processing circuits," *IEEE Transactions on Very Large Scale Integration (VLSI) Systems*, vol. 27, no. 10, pp. 2423–2433, 2019.
- [43] K. D. Abeyrathna, A. A. O. Abouzeid, B. Bhattarai, C. Giri, S. Glimsdal, O.-C. Granmo, L. Jiao, R. Saha, J. Sharma, S. A. Tunheim, and X. Zhang, "Building concise logical patterns by constraining Tsetlin machine clause size," in *Proceedings of the Thirty-Second International Joint Conference on Artificial Intelligence, IJCAI-23*, E. Elkind, Ed. International Joint Conferences on Artificial Intelligence Organization, 8 2023, pp. 3395–3403, main Track. [Online]. Available: <https://doi.org/10.24963/ijcai.2023/378>

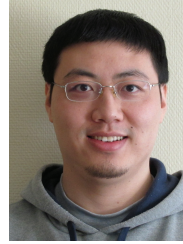


Svein Anders Tunheim is a PhD research fellow at the University of Agder at Centre for Artificial Intelligence Research (CAIR). He completed his MSc degree in Electrical Engineering at The Norwegian University of Science and Technology (NTNU) in 1991. From 1992 to 1996 he worked as research scientist at SI (Senter for Industriforskning) and SINTEF within the field of mixed-signal integrated circuits (ICs). He was co-founder and Chief Technology Officer at Chipcon, a global supplier of low-power radio frequency ICs and radio protocols. From

2006 to 2008 he worked at Texas Instruments Norway as Technical Director for the Low Power Wireless product line. Currently, at CAIR, he is working on low-power hardware implementations of machine learning systems based on the Tsetlin Machine. He is a Senior Member of IEEE.

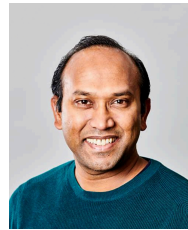


Yujin Zheng is a PhD candidate in the Microsystems Research Group at Newcastle University. She received her Master's degree in Microelectronics at Newcastle University and a Bachelor's in Applied Electronics from the University of Electronic Science and Technology of China (UESTC). Yujin was a senior board-level hardware engineer in China. She is currently working on ASIC implementation for hardware security.



Lei Jiao received the B.E. degree in telecommunications engineering from Hunan University, Changsha, China, in 2005, the M.E. degree in communication and information system from Shandong University, Jinan, China, in 2008, and the Ph.D. degree in information and communication technology from the University of Agder (UiA), Norway, in 2012. He is currently working as a Professor with the Department of Information and Communication Technology, UiA. His research interests include reinforcement learning, Tsetlin machine, resource allocation

and performance evaluation for communication and energy systems.



Rishad Shafik is a Professor in Electronic Systems within the School of Engineering, Newcastle University, UK. Professor Shafik received his PhD, and MSc (with distinction) degrees from Southampton in 2010, and 2005; and BSc (with distinction) from the IUT, Bangladesh in 2001. He is one of the editors of the Springer USA book "Energy-efficient Fault-tolerant Systems". He is also author/co-author of 200+ IEEE/ACM peer-reviewed articles, with 4 best paper nominations and 3 best paper/poster awards. He recently chaired multiple international conferences/symposiums, UKCAS2020, ISCAS2025, ISTM2022; guest edited a special theme issue in Royal Society Philosophical Transactions A; he is currently chairing 2nd IEEE SAS, 2025. His research interests include hardware/software co-design for energy-efficiency and autonomy.



Alex Yakovlev received the Ph.D. degree from the St. Petersburg Electrical Engineering Institute, St. Petersburg, USSR, in 1982, and D.Sc. from Newcastle University, UK, in 2006. He is currently a Professor of Computer Systems Design, who founded and leads the Microsystems Research Group, and co-founded the Asynchronous Systems Laboratory, Newcastle University. He was awarded an EPSRC Dream Fellowship from 2011 to 2013. He has published more than 500 articles in various journals and conferences, in the area of concurrent

and asynchronous systems, with several best paper awards and nominations. He has chaired organizational committees of major international conferences. He has been principal investigator on more than 30 research grants and supervised over 70 Ph.D. students. He is a fellow of the Royal Academy of Engineering, UK.



Ole-Christoffer Granmo is the Founding Director of the Centre for Artificial Intelligence Research (CAIR), University of Agder, Norway. He obtained his master's degree in 1999 and the PhD degree in 2004, both from the University of Oslo, Norway. In 2018 he created the Tsetlin machine, for which he was awarded the AI researcher of the decade by the Norwegian Artificial Intelligence Consortium (NORA) in 2022. Dr. Granmo has authored more than 160 refereed papers with eight paper awards within machine learning, encompassing learning automata, bandit algorithms, Tsetlin machines, Bayesian reasoning, reinforcement learning, and computational linguistics. He has further coordinated 7+ research projects and graduated 55+ master- and nine PhD students. Dr. Granmo is also a co-founder of NORA. Apart from his academic endeavours, he co-founded the companies Anzyz Technologies AS and Tsense Intelligent Healthcare AS.